

Acute and non-resolving inflammation associate with oxidative injury after human spinal cord injury

 Tobias Zrzavy,¹ Carmen Schwaiger,² Isabella Wimmer,¹ Thomas Berger,¹ Jan Bauer,³ Oleg Butovsky,^{4,5} Jan M. Schwab,^{6,7,8,9} Hans Lassmann³ and  Romana Höftberger²

Traumatic spinal cord injury is a devastating insult followed by progressive cord atrophy and neurodegeneration. Dysregulated or non-resolving inflammatory processes can disturb neuronal homeostasis and drive neurodegeneration. Here, we provide an in-depth characterization of innate and adaptive inflammatory responses as well as oxidative tissue injury in human traumatic spinal cord injury lesions compared to non-traumatic control cords. In the lesion core, microglia were rapidly lost while intermediate (co-expressing pro- as well as anti-inflammatory molecules) blood-borne macrophages dominated. In contrast, in the surrounding rim, TMEM119⁺ microglia numbers were maintained through local proliferation and demonstrated a predominantly pro-inflammatory phenotype. Lymphocyte numbers were low and mainly consisted of CD8⁺ T cells. Only in a subpopulation of patients, CD138⁺/IgG⁺ plasma cells were detected, which could serve as candidate cellular sources for a developing humoral immunity. Oxidative neuronal cell body and axonal injury was visualized by intracellular accumulation of amyloid precursor protein (APP) and oxidized phospholipids (e06) and occurred early within the lesion core and declined over time. In contrast, within the surrounding rim, pronounced APP⁺/e06⁺ axon-dendritic injury of neurons was detected, which remained significantly elevated up to months/years, thus providing mechanistic evidence for ongoing neuronal damage long after initial trauma. Dynamic and sustained neurotoxicity after human spinal cord injury might be a substantial contributor to (i) an impaired response to rehabilitation; (ii) overall failure of recovery; or (iii) late loss of recovered function (neuro-worsening/degeneration).

- 1 Department of Neurology, Medical University of Vienna, Vienna, Austria
- 2 Division of Neuropathology and Neurochemistry, Department of Neurology, Medical University of Vienna, Vienna, Austria
- 3 Center for Brain Research, Medical University of Vienna, Austria
- 4 Ann Romney Center for Neurologic Diseases, Department of Neurology, Brigham and Women's Hospital, Harvard Medical School, Boston, MA, USA
- 5 Evergrande Center for Immunologic Diseases, Brigham and Women's Hospital, Harvard Medical School, Boston, MA, USA
- 6 The Belford Center for Spinal Cord Injury, The Ohio State University, Columbus, OH 43210, USA
- 7 Department of Neurology, The Ohio State University, Columbus, OH 43210, USA
- 8 Department of Physical Medicine & Rehabilitation, The Ohio State University, Columbus, OH 43210, USA
- 9 Department of Neuroscience, The Ohio State University, Columbus, OH 43210, USA

Correspondence to: Romana Höftberger
Division of Neuropathology and Neurochemistry, Department of Neurology, Medical University of Vienna, Vienna, Austria
E-mail: romana.hoeftberger@meduniwien.ac.at

Keywords: oxidative injury; adaptive immunity; microglia; blood-derived macrophages; spinal cord injury

Abbreviations: PMN = polymorphonuclear neutrophil; SCI = spinal cord injury

Received March 27, 2020. Revised July 8, 2020. Accepted August 11, 2020. Advance access publication December 1, 2020

© The Author(s) (2020). Published by Oxford University Press on behalf of the Guarantors of Brain.

This is an Open Access article distributed under the terms of the Creative Commons Attribution Non-Commercial License (<http://creativecommons.org/licenses/by-nc/4.0/>), which permits non-commercial re-use, distribution, and reproduction in any medium, provided the original work is properly cited. For commercial re-use, please contact journals.permissions@oup.com

Introduction

Traumatic spinal cord injury (SCI) is a devastating condition with a substantial economic burden impacting on the physical and psychological well-being of patients (Ahuja *et al.*, 2017; James *et al.*, 2019). The initial mechanical injury is not only followed by classical secondary injury (Orr and Gensel, 2018) but also by long-standing progressive neurodegeneration (Freund *et al.*, 2013; Ziegler *et al.*, 2018) as reported for a subpopulation of traumatic SCI patients presenting with continued worsening of neurological functions even >6 months post-injury (Marino *et al.*, 1999; Kirshblum *et al.*, 2004). Evidence from experimental studies suggests that limiting pro-inflammatory bystander damage can improve SCI outcome (Gris *et al.*, 2004; Kerr *et al.*, 2008; David *et al.*, 2012; Ramer *et al.*, 2014).

Within the first hours to days after the insult in both humans and experimental animals, polymorphonuclear neutrophils (PMNs) accumulate at the lesion site and peak within the first 24 h (Taoka *et al.*, 1997; Fleming *et al.*, 2006; Beck *et al.*, 2010). Microglia activation and monocyte/macrophage infiltration follow during the first days and their numbers remain elevated up to months post-SCI (Fleming *et al.*, 2006; Pruss *et al.*, 2011). Similar patterns have been described for T cells in human SCI (Fleming *et al.*, 2006), although significant species differences between mice, rats and humans have been described in regard to lymphocyte composition as well as spatiotemporal patterns (Sroga *et al.*, 2003). Although a potential peripheral autoimmune response has been discussed in human SCI (Zajarias-Fainsod *et al.*, 2012), lesion-associated B cells have not been observed in the only available neuropathological assessment of human SCI thus far (Fleming *et al.*, 2006). This is in contrast to experimental SCI models, for which B cell accumulation and plasma cell conversion with concomitant IgG autoantibody production has already been shown (Ankeny *et al.*, 2006, 2009).

Microglia and CNS-infiltrating blood-derived macrophages arise from two ontogenetically distinct populations and can adopt a gradient from a pro-inflammatory phenotype associated with cytotoxicity and a potential beneficial anti-inflammatory phenotype (Kigerl *et al.*, 2009; Ginhoux *et al.*, 2010; Kroner *et al.*, 2014; Ransohoff, 2016). In experimental SCI models, an M1 pro-inflammatory polarization of microglia/macrophages prevails (Kigerl *et al.*, 2009). So far, polarization patterns in human SCI cases have not been studied. The distinction between purely M1 and M2 phenotypes is anyhow oversimplified and not advisable for *in vivo* studies (Ransohoff, 2016; Zrzavy *et al.*, 2017, 2018). Instead, microglia/macrophages should be characterized according to their functional properties, e.g. by means of the homeostatic marker P2RY12, which is lost in a pathological CNS environment (Fleming *et al.*, 2006; Beck *et al.*, 2010; Krasemann *et al.*, 2017). Under neuroinflammatory conditions, microglia and macrophages dominantly express

molecules involved in the production of reactive oxygen species. Oxidative neuronal injury is triggered by reactive oxygen species resulting in lipid peroxidation and intracellular accumulation of oxidized phospholipids. Oxidative neuronal injury is well documented for human CNS injury and associated with activated microglia and macrophages (Haider *et al.*, 2011; Jia *et al.*, 2012).

Most of our understanding of the inflammatory response after SCI derives from preclinical experiments, which do not always reflect the human CNS pathophysiology (Dirnagl, 2014; Schuh *et al.*, 2014). Detailed information on human traumatic SCI, however, is sparse and molecular mechanisms contributing to delayed neurodegeneration are likewise unknown, which poses a fundamental void in our understanding of the pathophysiology after human SCI. To fill in missing links, we performed a systematic analysis of (i) the recruitment of leucocytes into human SCI lesions; and (ii) the spatiotemporal heterogeneity of microglia and macrophages by applying a validated panel of functional markers. Moreover, we characterized the kinetics of oxidative tissue injury by using oxidized lipids as validated and established marker for neuronal cell body and axonal injury (Haider *et al.*, 2011; Friese *et al.*, 2014).

Material and methods

Sample characterization

Our study was performed using an archival collection of spinal cord autopsy tissues derived from 22 patients with traumatic SCI and five non-traumatic control patients; all collected during the past decades in the archive of the Division of Neuropathology and Neurochemistry, Department of Neurology, Medical University of Vienna. All available medical records, laboratory charts and autopsy charts were screened. Non-traumatic control cases were comprehensively examined for any pathological alterations in the white and grey matter, particularly inflammatory infiltrates and signs of tissue injury, for which tissue sections were routinely stained with haematoxylin and eosin, Luxol fast blue and Bielschowsky silver impregnation. Patient demographics, time of death post-SCI and lesion level are summarized in Table 1. The study was approved by the ethics committee of the Medical University of Vienna (EK. Nr.: 1454/2018 and 1636/2019).

Immunohistochemistry

Immunohistochemistry was performed on formalin-fixed paraffin-embedded tissue sections with a biotin/avidin detection system as described in detail before (Bauer and Lassmann, 2016) using primary antibodies and respective antigen retrieval methods as listed in Supplementary Table 1. For lymphocyte characterization, we used antibodies targeting CD3 (T cells), CD4 (MHC class II-restricted T cells),

Table 1 Clinical demographics

Case	Level	Cause	Days post-injury	Cause of death	Age	Sex	Type of injury
SCI-1	Th	Gun shot	< 1	Cardiovascular failure	33	M	Massive compression
SCI-2	C	Fall	1	Cardiovascular failure	79	M	Contusion/cyst
SCI-3	C	Fall	2	Respiratory insufficiency	30	M	Contusion/cyst
SCI-4	C	Fall	2	Pulmonary embolism	79	F	Massive compression
SCI-5	C	Fall	4	Cardiovascular failure	53	M	Contusion/cyst
SCI-6	C	Fall	4	Cardiovascular failure	75	F	Contusion/cyst
SCI-7	C	Fall	5	Pulmonary embolism	50	M	Contusion/cyst
SCI-8	TH	Massive prolapsed disc	13	Pulmonary embolism	35	F	Massive compression
SCI-9	C	Fall	14	Unknown	45	F	Contusion/cyst
SCI-10	C	Fall	15	Cardiovascular failure	37	M	Contusion/cyst
SCI-11	C	Fall	19	Unknown	15	M	Contusion/cyst
SCI-12	C	Fall	18	Cardiovascular failure	71	M	Contusion/cyst
SCI-13	L	Car accident	18	Renal failure	19	M	Contusion/cyst
SCI-14	C	Fall	25	Respiratory insufficiency	39	M	Massive compression
SCI-15	C	Fall	36	Respiratory insufficiency	22	M	Contusion/cyst
SCI-16	C	Fall	48	Pulmonary oedema	80	M	Contusion/cyst
SCI-17	C	Fall	89	Hepatorenal failure	65	M	Contusion/cyst
SCI-18	C	Fall	91	Pulmonary embolism	61	M	Contusion/cyst
SCI-19	TH	Car accident	210	Pulmonary oedema	34	F	Contusion/cyst
SCI-20	C	Car accident	352	Cardiovascular failure	24	F	Contusion/cyst
SCI-21	C	Massive prolapsed disc	365	Cardiovascular failure	56	M	Contusion/cyst
SCI-22	C	Fall	413	Cardiovascular failure	58	M	Contusion/cyst
CO-1	C			Cardiovascular failure	53	F	
CO-2	C			Renal failure	40	M	
CO-3	C			Hepatic failure	73	M	
CO-4	C			Cardiovascular failure	70	F	
CO-5	C			Hepatic failure	32	M	

C = cervical; F = female; L = lumbar; M = male; Th = thoracic.

CD8 (MHC class I-restricted T cells), CD20 (B cells), CD79a (B cells and plasma cells) and CD138 (plasma cells). Lymphocytes were distinguished from macrophages, which can express CD4 or CD8 as well, by morphological criteria and a lack of CD68 expression. C9neo staining was used to identify complement-mediated tissue injury (Bien *et al.*, 2012). Granulocytes were detected by their characteristic appearance (segmented cell nuclei) in tissue sections stained with haematoxylin and eosin. For the characterization of myeloid cells, Iba-1 was used as a general microglia/macrophage marker; TMEM119 and P2RY12 were used as microglia-specific markers. TMEM119 is a transmembrane protein with unknown function expressed on microglia, but not on recruited myeloid cells in humans and rodents (Butovsky *et al.*, 2014; Bennett *et al.*, 2016). During microglia activation, TMEM119 expression is downregulated; however, a residual level is preserved on the surface (Satoh *et al.*, 2016). Resting microglia were identified using P2RY12, which is rapidly lost upon activation in experimental models of CNS inflammation or neurodegeneration (Krasemann *et al.*, 2017; Zrzavy *et al.*, 2017). CD68 was used to detect phagocytic activity; HLA-DR and CD86 were used to identify cells involved in antigen presentation, processing and co-stimulation. Furthermore, p22phox (NADPH oxidase) and inducible nitric oxide synthase (iNOS) were used as markers for oxidative activation and signs of

oxidative tissue injury. Anti-e06 antibodies were applied to detect oxidative injury (intracellular loading with oxidized phospholipids) in neurons (Haider *et al.*, 2016). As prototypical anti-inflammatory markers, expression of the haemoglobin-haptoglobin receptor CD163 and the mannose receptor CD206 were investigated (Zrzavy *et al.*, 2018). Moreover, staining for the pro-inflammatory cytokines interleukin-1 β (IL-1 β) and interleukin-18 (IL-18) as well as the anti-inflammatory cytokines interleukin-10 (IL-10) and transforming growth factor beta (TGF- β) were performed (Machado-Santos *et al.*, 2018; Tröscher *et al.*, 2019). All markers have already been extensively characterized regarding their reliability and expression patterns in human autopsy material of lymphatic tissue (Zrzavy *et al.*, 2017). For control, immunohistochemistry was performed by omitting of primary antibodies and by using normal rat and goat serum or isotype-matched monoclonal antibodies.

For double stainings using primary antibodies derived from different species, the same antigen retrieval techniques were applied as described in Supplementary Table 1. Visualization was performed by using (i) alkaline phosphatase-conjugated secondary antibodies for subsequent development with Fast Blue BB salt; and (ii) biotinylated secondary antibodies and peroxidase-conjugated streptavidin for subsequent development with amino ethyl carbazole (AEC). For double stainings using primary antibodies derived from

same species (TMEM119, p22phox, APP, e06), heat-induced epitope retrieval was performed in between the separate antibody incubations and subsequent immunohistochemical detection reactions according to [Bauer and Lassmann \(2016\)](#).

Immunofluorescence

For fluorescence double or triple stainings, with two antibodies from the same species, extensive heat-induced epitope retrieval in between the subsequent immunohistochemical reactions was performed. After deparaffination and blocking of non-specific binding, the first round of antigen retrieval ([Supplementary Table 1](#)) was done and tissue sections were incubated with primary antibodies against Iba-1, P2RY12 or IL-18. This was followed by incubation with biotinylated anti-rabbit antibody and avidin peroxidase as well as catalysed signal amplification with biotinylated tyramine ([Bauer and Lassmann, 2016](#)). Then, a second round of antigen retrieval (30 min; EDTA buffer pH 9) was done, followed by incubation of tissue sections with Cy2- or Cy3-conjugated streptavidin. Thereafter, the second round of primary antibodies (anti-TMEM119, anti-GFAP or combinations from different species) were applied and visualized by subsequent incubation with Cy3 or Cy5-conjugated anti-rabbit, anti-goat or anti-mouse secondary antibodies ([Tröscher et al., 2019](#); [Zrzavy et al., 2019](#)). Finally, sections were mounted with ProlongTM Gold antifade mountant (Thermo Fisher Scientific, P36930) and visualized with a confocal laser microscope (Leica SP5, Austria).

Turnbull blue staining

3,3'-Diaminobenzidine tetrahydrochloride hydrate (DAB)-enhanced Turnbull's blue (TBB) staining for the detection of non-haem iron was done as described ([Hametner et al., 2013](#)).

Quantitative assessment

Regions of interest included the lesion core ('core') as well as the directly surrounding tissue margin ('rim') ([Fig. 1](#)). The core region corresponds to the definition of 'Zone 1' and the rim region to the definition of 'Zone 2' as described previously ([Fleming et al., 2006](#)). The spinal cords were classified into the following stages (time windows) after SCI displaying consistent histopathology: (stage I) 1–3 days post-SCI ($n = 4$); (stage II) 4–21 days post-SCI ($n = 9$); (stage III) 21–90 days post-SCI ($n = 4$); and (stage IV) 90 days to 1.5 years post-SCI ($n = 5$) compared to controls ($n = 5$). For the quantitative evaluation of microglia/macrophages, sections were overlaid by a morphometric grid (0.2256 mm²) placed within the ocular lens and two to three fields per region of interest were selected. Cells expressing the respective marker were manually counted and the values are expressed as cell counts per square millimetre. For quantification of lymphocytes, a morphometric grid within the ocular lens

was used as well and inflammatory cell numbers were manually counted in 5–20 fields of 0.2256 mm² per region of interest spanning the entire lesion. The number of T cells and B cells were counted separately for perivascular and parenchymal areas and were pooled afterwards.

Digital optical densitometry was performed for quantification of oxidized phospholipids (e06 immunoreactivity) according to a previously published protocol ([Hametner et al., 2013](#)). This marker was quantified by calculating the positive DAB signal area fraction using ImageJ. One to two images per region of interest were taken with standardized acquisition settings. For digital removal of haematoxylin counterstaining, a colour deconvolution plugin (freeware kindly provided by A. C. Ruifrok, NIH) was run. Further RGB images were converted into 8-bit greyscale images and inverted. A threshold was set, which was kept constant between analyses; subsequently, the area fraction of the resulting images was calculated.

Statistical analysis

Statistical analysis was performed with IBM SPSS 20.0.0 (SPSS Inc, Chicago, IL, USA) and GraphPad Prism[®] v6.01. Because of uneven distribution of our data, statistical analysis was performed with non-parametric tests. Descriptive analysis included median value and range. Differences between two groups were assessed with Wilcoxon Mann-Whitney U-test. In case of multiple testing, significant values were corrected with the Bonferroni-Holm procedure. The reported *P*-values are results of two-sided tests. A *P*-value ≤ 0.05 was considered statistically significant.

Data availability

Data can be made available from the corresponding author upon reasonable request and after approval from the ethics review board at the Medical University of Vienna.

Results

For the analysis of inflammatory and degenerative cascades following traumatic SCI, we examined an archival tissue collection of 22 traumatic SCI and five non-traumatic control cases ([Table 1](#)). The mean age of the SCI cohort was 48.1 years (range 15–80 years), which was slightly younger than the control cohort (53.4 years, range 32–73 years). The gender distribution ratio was 16:6 (male: female) in the spinal injury cohort, which matches epidemiological data ([Ahuja et al., 2017](#)), and 3:2 (male: female) in the control group. All analysed tissue blocks contained the actual impact zone of SCI. Since (i) it is impossible to reliably distinguish between grey and white matter in the case of severe SCI; and (ii) we did not see significant differences in microglia numbers between normal spinal cord grey and white matter (data not shown), we did not differentiate between the two areas in further analyses. Putative control cases were solely admitted

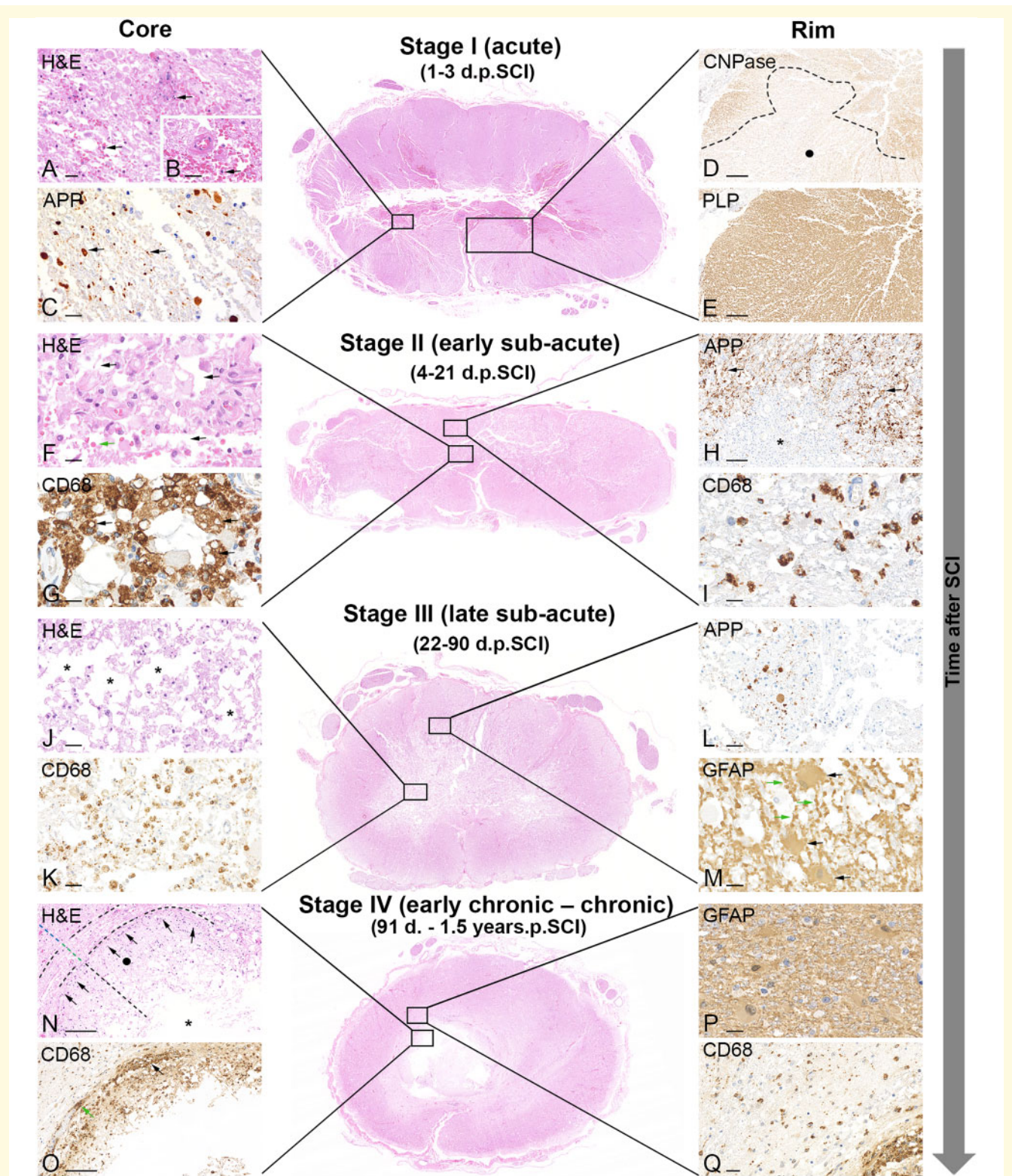


Figure 1 Spatiotemporal characterization of neuropathological features in human SCI lesions. The sequence of neuropathological alterations was grouped into four stages (I–IV). An overview of the progressive lesion evolution is illustrated by haematoxylin and eosin (H&E)-stained spinal cord cross-sections (middle row) accompanied by higher-resolution details of the corresponding lesion core (left) and surrounding rim (right). Anterior spinal cord is facing downwards, while dorsal cord is directed upwards. Stage I (1–3 days post-SCI): (A) Distortion and disruption of parenchyma and inherent vessels with ensuing haemorrhage and leukodiapedesis (extravasation, arrows) in the lesion core. Hyperpolarized red blood cells are detected outside of the neurovascular unit in a radial manner in close vicinity to the damaged vessels (B). Abundant swollen hypertrophic β -APP⁺ axonal spheroids (black arrow) indicate axonal injury. These ballooned retraction bulbs indicate severe cytoskeletal disruption and are intermingled with β -APP⁺ axons displaying features (dotted segregated β -APP⁺ alignments; green arrow) in line

(continued)

to the control cohort if pathological changes, particularly inflammatory infiltrates and signs of tissue injury, which would have been detectable in haematoxylin and eosin staining, Luxol fast blue myelin staining and Bielschowsky silver impregnations, could be fully excluded.

Different spatiotemporal dynamics of neuropathology evolve after human spinal cord injury

For a rough categorization, the sequence of neuropathological alterations after traumatic SCI, which include inflammation, neurodegeneration and tissue damage, can be grouped into four stages (I–IV): SCI of stage I (1–3 days post-SCI) was characterized by distortion and disruption of parenchyma integrity, haemorrhage, and leukodiapedesis (extravasation) in the lesion core (Fig. 1A and B) with abundant β -APP⁺ axonal spheroids indicating axonal injury (axonal blebbing) (Fig. 1C). In the lesion-surrounding white matter, commencing myelin damage (demyelination) with early 2',3'-cyclic-nucleotide 3'-phosphodiesterase (CNPase) loss was evident (Fig. 1D); expression of proteolipid protein (PLP) was still preserved (Fig. 1E). Injured spinal cords of stage II (4–21 days post-SCI) demonstrated tissue necrosis within the lesion core with typical spongiotic tissue changes (Fig. 1F) concomitant with ongoing debris removal evidenced by large numbers of CD68⁺ macrophages containing large lysosomal vacuoles (Fig. 1G). Within the lesion rim, abundant β -APP⁺ axonal spheroids with various elongations ('axonal varicosities') (Fig. 1H) and scattered CD68⁺ macrophages (Fig. 1I) were present. Stage III (21–90 days post-SCI) was characterized by progressive spongiotic changes

with numerous CD68⁺ macrophages in the lesion core (Fig. 1J and K). However, in comparison with stage II, the number of CD68⁺ macrophages had already subsided. In the lesion rim, remaining axonal spheroids were surrounded by reactive gliosis composed of hypertrophic activated GFAP⁺ astrocytes (Fig. 1L and M), which extended vascular end-feet with pronounced bouton-type appearance in order to support vascular integrity (stabilization of the neurovascular unit) (Fig. 1M). Finally, stage IV (90 days to 1.5 years post-SCI) demonstrated cystic cavitation (syrinx) in the lesion centre. This scar was surrounded by a hypercellular rim (Fig. 1N) containing non-resolving, activated CD68⁺ macrophages. (Fig. 1O). They also formed clusters in Virchow-Robin-like spaces pointing to a chronic immunological activation (Fig. 1O). The lesion rim showed massive reactive GFAP⁺ gliosis and a remainder of evenly distributed CD68⁺ macrophages was still present (Fig. 1P and Q). Spinal cord tissue from controls did not contain any pathological changes (not shown). We further extended the basic spatiotemporal characterization of human traumatic SCI lesions with more detailed analyses of cellular compositions and activation patterns as well as of oxidative tissue injury.

Polymorphonuclear neutrophils

PMNs were absent in non-traumatic control spinal cords (Figs 2A and 3A). After traumatic SCI, they were readily present, peaked within the first 3 days after injury in the lesion core ($P = 0.032$) (Figs 1A, B and 2A) and were also detectable in some cases within the lesion rim (Fig. 3A). The number of PMNs declined during the first 3 weeks post-SCI and they were not observed at any later time points

Figure 1 Continued

with axonal fragmentation (Williams *et al.*, 2014) (C). (D) In the lesion-surrounding white matter, there is evidence of beginning myelin damage (demyelination) with early CNPase loss (black dot), while (E) PLP still remains preserved. Stage II (4–21 days post-SCI): Tissue necrosis with massive, macrophage infiltration into the lesion core. Emerging spongiotic tissue changes (arrows) reflect actively ongoing debris removal (F) evidenced by CD68⁺ macrophages containing large lysosomal vacuoles (arrows) (G). Non-phagocytosed extravasated erythrocytes are, however, still present (F, green arrow). (H) A demarcation between lesion core (asterisk) and lesion rim is visible since areas of impaired axoplasmic transport in the rim show massive accumulation of β -APP⁺ axonal spheroids. Hypertrophic retraction bulbs (arrow) are detectable in close juxtaposition to the lesion. (I) Density of CD68⁺ monocytes/macrophages is lower and the lysosomes smaller. Stage III (22–90 days post-SCI): (J and K) Progressive, enlarged spongiotic changes (asterisks) emerging towards the beginning demarcation of a cystic cavitation in the surrounding rim, remaining axonal β -APP⁺ spheroids (L) are still present; however, in reduced numbers compared to the preceding stage II. Signs of axonal fragmentation are no longer detected. (M) β -APP⁺ axons are surrounded by reactive gliosis composed of hypertrophic activated GFAP⁺ astrocytes reflective of matured lesion organization (arrows). Hypertrophic GFAP⁺ astrocytes extend vascular end-feet with pronounced bouton-type appearance (green arrows) to support vascular integrity (stabilization of the neurovascular unit) (M). Stage IV (22–90 days post-SCI): (N) Cystic cavitation (syrinx) and surrounding scar formation is composed of an hypercellular rim, demonstrating declining cell numbers (gradient, black dot), further extending towards the core (asterisk) into an area of extracellular matrix deposition characterized by hypocellularity (black dot). (O) The scar contains non-resolving, activated CD68⁺ macrophages, which form an inflammatory 'layer' confined to the immediate border between the hypercellular and hypocellular regions with declining cell numbers towards the syrinx core. Non-resolving lipid-laden (foamy) CD68⁺ macrophages form compartmentalized clusters 'locked' into the immediate scar (arrow). CD68⁺ monocytes/macrophages also form clusters in Virchow-Robin-like spaces (green arrow) pointing to a chronic immunological activation or drainage (Wardlaw *et al.*, 2020). (P and Q) The rim illustrates massive reactive GFAP⁺ astroglial gliosis with some remaining evenly distributed CD68⁺ macrophages. Of note, also the rim represents an area of higher immune alertness characterized by higher numbers of CD68⁺ myeloid cells even until chronic stages. Spinal cord tissue from controls did not contain any pathological changes (not shown). Scale bars = 25 μ m in A–C, F, G, I–M, P and Q; 250 μ m in D and E; and 125 μ m in H, N and O.

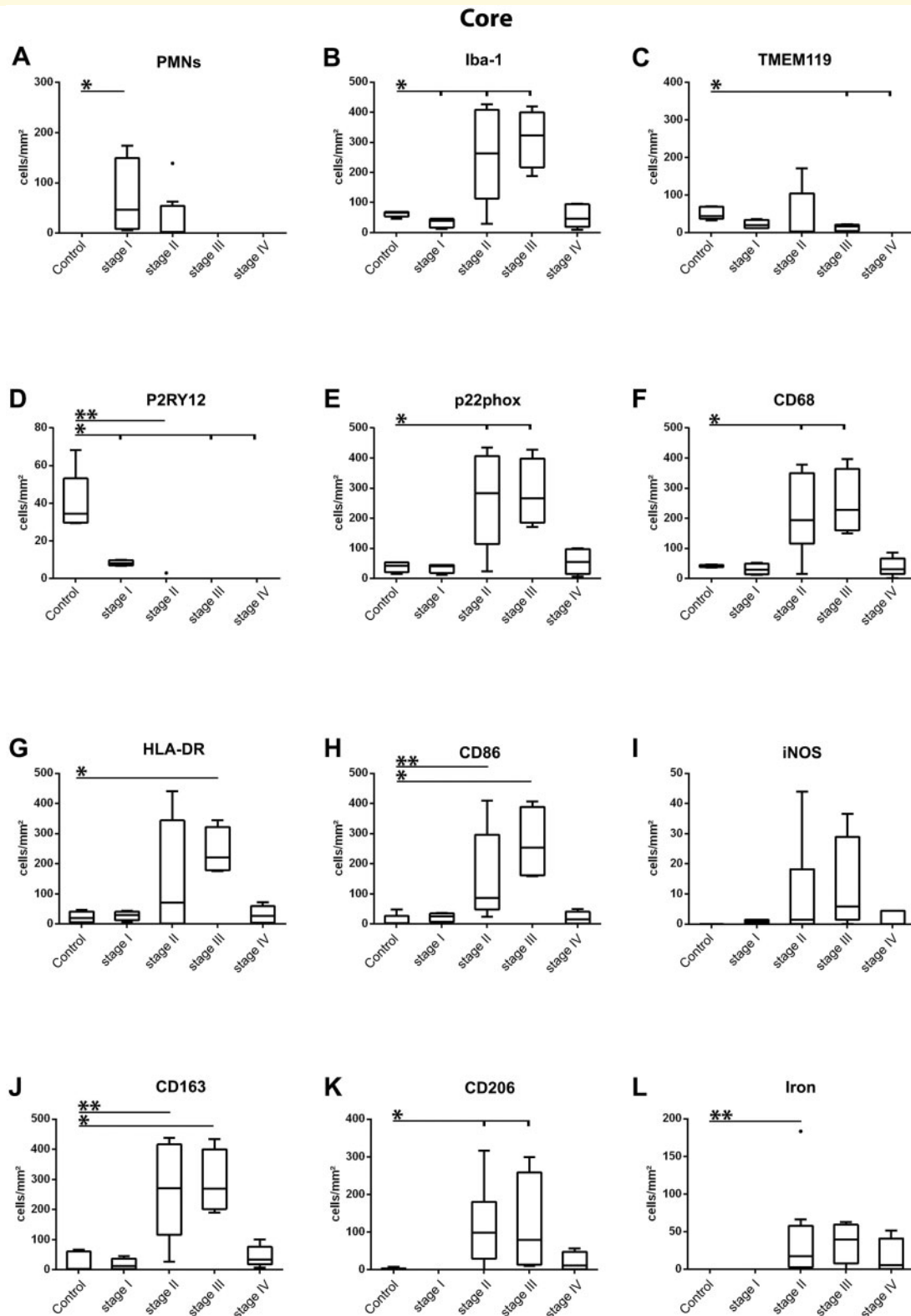


Figure 2 Quantitative analysis of cellular markers in the spinal cord lesion core. Quantitation of PMNs and various microglia/macrophage marker expression in the core of SCI lesions at different lesion stages (I–IV) as well as in non-traumatic control tissue. Data represent actual numbers of cells/mm². (A) PMNs counted in haematoxylin and eosin staining, (B) pan-microglia/macrophage marker Iba-1, (C) the microglia-specific marker TMEM119, (D) the ‘homeostatic’ microglia marker P2RY12; and the microglia activation markers (E) p22phox, (F) CD68, (G) HLA-DR, (H) CD86, (I) iNOS, (J) CD163, (K) CD206 and DAB-enhanced TBB staining for the detection of non-haem iron (L). **P* ≤ 0.05; ***P* ≤ 0.01; ****P* ≤ 0.001.

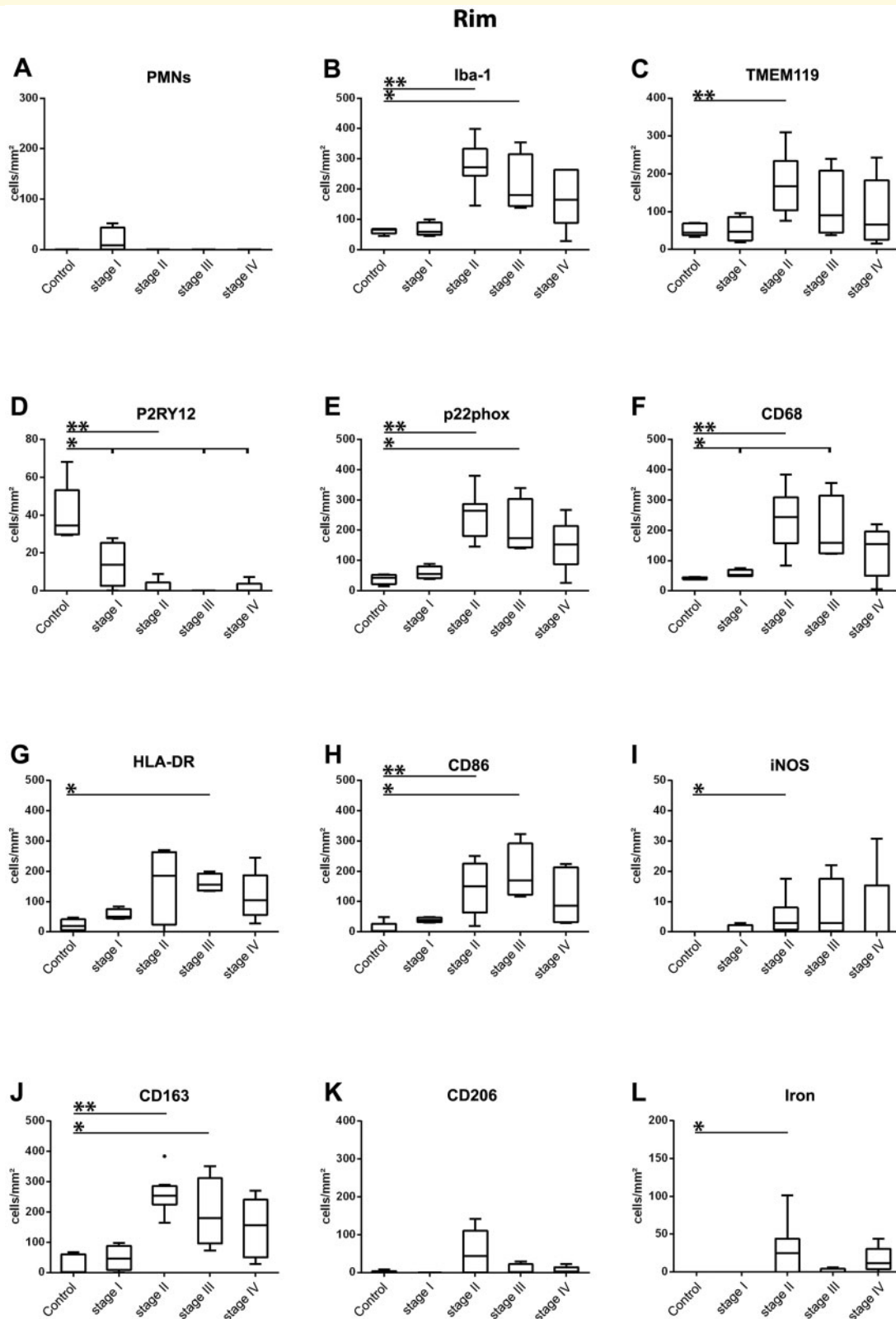


Figure 3 Quantitative analysis of cellular markers in the spinal cord lesion rim. Quantitation of PMNs and various microglia/macrophage marker expression in the core of SCI lesions at different lesion stages (I–IV) as well as in non-traumatic control tissue. Data represent actual numbers of cells/mm². **(A)** PMNs counted in haematoxylin and eosin staining, **(B)** pan-microglia/macrophage marker Iba-1, **(C)** the microglia-specific marker TMEM119, **(D)** the ‘homeostatic’ microglia marker P2RY12; and the microglia activation markers **(E)** p22phox, **(F)** CD68, **(G)** HLA-DR, **(H)** CD86, **(I)** iNOS, **(J)** CD163, **(K)** CD206 and DAB-enhanced Turnbull Blue (TBB) staining for the detection of non-haem iron **(L)**. **P* < 0.05; ***P* < 0.01; ****P* < 0.001.

analysed. PMNs were located perivascularly; in some cases, they were detected in the parenchyma as well.

Microglia and blood-derived macrophages in the lesion core and surrounding lesion rim

In non-traumatic control patients, Iba-1⁺ cells exhibited a ramified microglia phenotype and co-expressed the microglia marker TMEM119 (Fig. 4A). Most of these TMEM119⁺ cells were positive for the homeostatic marker P2RY12 as well (Fig. 4B). In the necrotic core of stage I lesions, we detected a significant loss of Iba-1⁺ cells ($P = 0.032$), while their numbers remained constant in the surrounding rim (Figs 2B and 3B). The vast majority of Iba-1⁺ cells in both lesion core and rim were TMEM119⁺ (average 81% and 89%, respectively) (Figs 2C and 3C). At stage II, there was a massive increase of Iba-1⁺ cells within the lesion core as well as rim ($P = 0.019$ and $P = 0.002$, respectively) (Figs 2B and 3B). However, while 80% of Iba-1⁺ cells within the lesion rim were also TMEM119⁺, this number dropped to 10% within the lesion core. Morphologically, cells in the lesion core were characterized by an amoeboid shape i.e. oval to round cell bodies without processes (Fig. 4D and H). This indicates a substantial recruitment of peripheral TMEM119⁻ macrophages into the lesion core, while the increased numbers of Iba-1⁺ TMEM119⁺ cells within the lesion rim was mostly due to local microglia proliferation as shown by proliferating cell nuclear antigen (PCNA) expression (Fig. 4J) in 17% of TMEM119⁺ cells. At stage III, numbers of Iba-1⁺ cells were still significantly increased in both the lesion core and rim ($P = 0.32$ and $P = 0.32$, respectively) (Figs 2B and 3B). From stage II to stage III, there was a further decline of TMEM119⁺ co-expressing Iba-1⁺ cells to 5% in the lesion core; several months post-SCI (stage IV), we could not detect any more TMEM119⁺ cells in this area (Fig. 2C). In the rim, we observed that from stage II to IV, approximately half of Iba-1⁺ cells stably co-expressed TMEM119 (stage II, 80%; stage III, 49%; stage IV, 47%). Results show that microglia (Iba-1⁺ TMEM119⁺ cells) constituted a substantial proportion of myeloid cells in the edge during lesion maturation, while recruited blood-borne monocytes/macrophages (Iba-1⁺ TMEM119⁻ cells) dominated within the lesion core.

Differential patterns of microglia and macrophage activation

In the lesion core, a rapid and long-lasting loss of P2RY12 (homeostatic marker) expression on myeloid cells was detected (stage I, $P = 0.032$; stage II, $P = 0.002$; stage III, $P = 0.032$; stage IV, $P = 0.016$) (Figs 2D, 4E and F). A similar pattern was observed in the lesion rim; however, low numbers of P2RY12⁺ cells reappeared in some cases at later time points (stage IV) (Fig. 3D).

Within the core of tissue injury, a significant pro-inflammatory activation of myeloid cells, the vast majority of which

were TMEM119⁻, was detected by an upregulation of p22phox, CD86, MHC class II and CD68 expression (Figs 2E–H and 4). Numbers of iNOS⁺ myeloid cells also increased during stages II and III, albeit to much lower extents (Fig. 2I). Concomitant with pro-inflammatory markers, we also observed an increased expression of the anti-inflammatory markers CD163 and CD206, which reached a plateau within the first weeks post-injury (Fig. 2J and K). The co-occurrence of both pro- and anti-inflammatory molecules indicates that a substantial proportion of myeloid cells within the lesion core (mostly TMEM119⁻ cells) expressed an intermediate activation phenotype (Fig. 4K–P).

Within the lesion rim, the expression of the pro-inflammatory markers (i) was mostly detected on TMEM119⁺ myeloid cells (microglia); and (ii) peaked within the first 3 weeks (stage II) (Figs 3D–I, 4G and I). Contrary to the lesions core, the prominent pro-inflammatory patterns had not fully subsided at stage IV. Expression of CD163 was significantly elevated during the first weeks (stage II, $P = 0.002$; stage III, $P = 0.032$) (Figs 3J, 4Q and R). In contrast to CD163 and expression patterns observed in the lesion core, expression of the anti-inflammatory marker CD206 solely increased to non-significant extents at stage II and was rapidly lost thereafter. Notably, while 26% of Iba-1⁺ cells in the lesion core expressed CD206 at stage III, only 0.2% of Iba-1⁺ cells in the rim stained positive for CD206 (Fig. 4K–P). Iron-loaded macrophages were detected to a variable extent in the core and rim after 3 days (Figs 2L, 3L, 4S and T). Overall, our data show a time-dependent activation of microglia and macrophages, with a predominant pro-inflammatory expression pattern accentuated within the lesion rim and an intermediate pro- and anti-inflammatory phenotype within the lesion core.

Cytokine expression patterns

For the analysis of pro- and anti-inflammatory cytokine patterns, we investigated the expression of IL-1 β and IL-18 as well as IL-10 and TGF- β , respectively, in two representative cases of each SCI stage as well as in control cases (Fig. 5). IL-1 β and IL-10 immunoreactivity in myeloid cells was neither detectable in traumatic SCI nor control cases (data not shown). IL-18 was strongly expressed in microglia and macrophages in the lesion rim and core, respectively, throughout all SCI stages (Fig. 5A, B, F and G). Double labelling of IL-18 with the anti-inflammatory marker CD206 did not show any co-expression. (Fig. 5H and I); in SCI cases with particularly pronounced CD206 immunoreactivity, IL-18 expression was markedly reduced (Fig. 5I). TGF- β expression was only detected in astrocytes within the rim of lesion stages II and III and was absent in myeloid cells (Fig. 5C–E).

T cells, B cells, plasma cells and complement deposition

CD3⁺ T cells gradually infiltrated the lesion core over time (Fig. 6A, F and G). At the earliest time points in the lesion

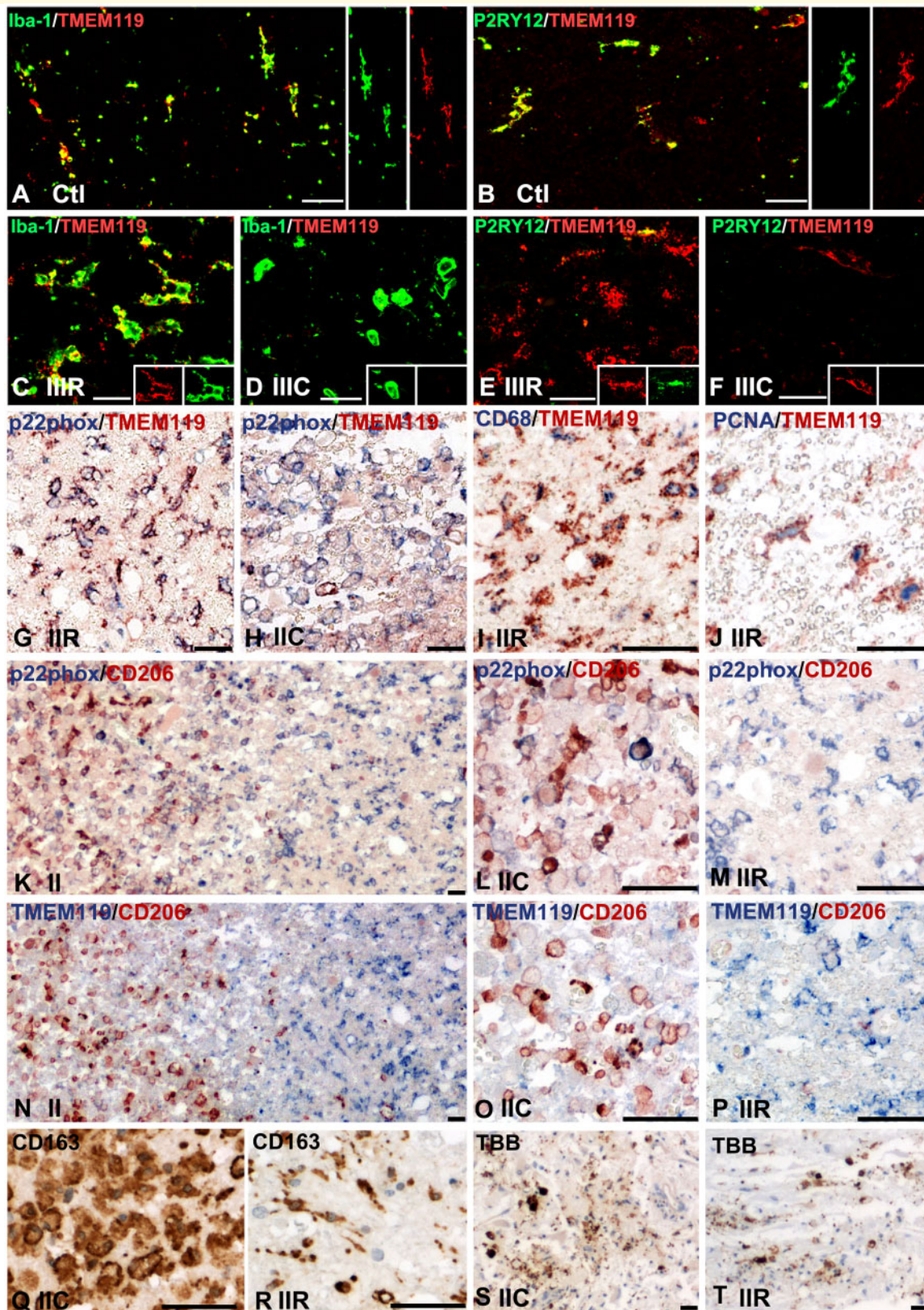


Figure 4 Loss of ‘homeostatic’ microglia within the lesion core and rim. Segregation of infiltrating monocytes towards the core while microglia persist within the rim. Distinct and faceted microglia and macrophage response to human traumatic SCI (A). Almost all microglia are double positive for Iba-1 (green) and TMEM119 (red) as well as (B) co-express P2RY12 (green) and TMEM119 (red) in the spinal cord of non-traumatic controls. (C) The rim of the lesions contains high numbers of Iba-1 (green) TMEM119 (red) double-positive cells, while (D) TMEM119⁺ (red) cells are massively reduced in the lesion core. Likewise, (E) sparse TMEM119 (red) P2RY12 (green) double-positive cells are

(continued)

core, T cells mainly located to perivascular spaces (Fig. 6F), while scattered parenchymal CD3⁺ T cells were detected at stages II and III and declined thereafter. T cells were not encountered close to neurons or oligodendrocytes but were diffusely distributed. The group of CD3⁺ T cells was mainly composed of CD8⁺ cells and only few CD4⁺ cells (Fig. 6B, H and I). In the lesion rim, the majority of T cells accumulated in the perivascular space, while only a low number of T cells was truly dispersed in the parenchyma. Overall, numbers of CD8⁺ T cells remained elevated until the chronic stage IV.

In most SCI cases, B cells were hardly present; if any, they were mainly found in perivascular spaces intermingled with other perivascular cells (Fig. 6C, D, J and K). Only in two cases, we observed a pronounced infiltration of CD79a⁺ B cells and CD138⁺ IgG⁺-producing plasma cells into the spinal cord parenchyma (Fig. 6L–N). In these two cases as well as five other patients (total *n* of SCI cohort = 22), we also observed deposition of activated complement (C9neo antigen) in the area of tissue necrosis (Fig. 6O). Our data show a predominance of CD8⁺ T cells in SCI and, at least in single cases, an infiltration of B cells.

Oxidative injury

In control spinal cords, immunoreactivity for the oxidized phospholipid marker e06 was only observed in lipofuscin granules (Fig. 7C). After SCI, e06 was detected either as lipofuscin or was diffusely distributed in the cytoplasm of neurons as well as dendrites and axons (Fig. 7D and E). E06⁺ neurons often presented with an injured phenotype such as axonal beading (Fig. 7J), an irregularly shaped plasma membrane (Fig. 7K) or central chromatolysis (Fig. 7L). Oxidized phospholipids readily accumulated within the lesion core and peaked within the first 3 weeks post-SCI (Fig. 7A). Thereafter, e06 immunoreactivity readily declined to control levels. The e06 immunoreactivity in the lesion core positively correlated with the appearance of granulocytes ($R = 0.426$, $P = 0.048$). In the lesion rim, oxidized phospholipids were most abundant in early stage II (maximum at Day 4: 2.71% area); contrary to the lesion core, e06⁺ oxidized phospholipid immunoreactivity remained significantly elevated even at the chronic stage IV ($P = 0.032$) (Fig. 7B and E–H). Our data suggest that oxidative injury has a long-term contribution to protracted injury and neurodegeneration after SCI.

Discussion

We here provide the first systematic characterization of spatial and temporal patterns of innate and adaptive immune responses as well as oxidative tissue injury after traumatic SCI in a large cohort of patients ($n = 22$). Our study identified inflammatory patterns evolving differently within the lesion core versus the surrounding rim. The core was characterized by and infiltration of blood-derived monocytes/macrophages adapting an intermediate pro- and anti-inflammatory phenotype, while locally proliferating pro-inflammatory microglia dominated within the rim. Tissue infiltrating T cells were mainly identified as CD8⁺ cells. In a small subpopulation of SCI patients, we identify parenchymal B cells and plasma cells as well; further, parts of the SCI cohort displayed activated complement deposits in areas of tissue necrosis. We provide evidence that oxidative injury occurs not only in the acute phase but also even months and to 1.5 years after the impact.

Neutrophils are temporally restricted to the acute or early-subacute spinal cord injury phase

PMNs constitute the first immune cell population, which accumulated in traumatic SCI lesions within the first 72 h and were rapidly cleared thereafter. PMNs assembled within the lesion core in areas of haemorrhagic transformation and subsequent haemorrhagic necrosis. This is in contrast to ischaemic CNS injury, in which PMNs remain mostly confined to the boundaries of the neurovascular unit and do not actively infiltrate the lesioned parenchyma (Enzmann *et al.*, 2013; Zrzavy *et al.*, 2018). For SCI, it still remains unclear whether PMNs actively infiltrate the tissue because of chemotactic cues or are passively shuttled into the tissue along with extravasating blood. Generally, PMN infiltration oftentimes leads to subsequent cytotoxic tissue damage due to excessive cytokine and prostaglandin release, oxidative burst and release of toxic granules (Bao *et al.*, 2004, 2008; Dinkel *et al.*, 2004; Gris *et al.*, 2004; Nguyen *et al.*, 2007). Similarly, we observed within our SCI cohort a significant association between the presence of PMNs and the detection of e06⁺ oxidative neuronal injury in the lesion core. Taken

Figure 4 Continued

still detectable in the rim, while (F) they are completely lost in the lesion core. In the lesion rim, the majority of microglia (TMEM119⁺ cells; red), expresses pro-inflammatory markers e.g. (G) p22phox (blue) (stage II) or (I) the phagocytosis-associated marker CD68 (blue); within the lesion core, hardly any myeloid cells expressing pro-inflammatory markers, e.g. (H) p22phox, co-express the microglia marker TMEM119. (J) Many microglia (TMEM119⁺, red) within the rim display nuclear co-expression of the proliferation marker proliferating cell nuclear antigen (PCNA; blue). (K) An example of an SCI lesion; within the core (left side), numerous pro-inflammatory (p22phox; blue) and anti-inflammatory (CD206; red) double-positive macrophages are present, whereas pro-inflammatory activation predominates within the rim (right side). (L and M) Higher magnification of lesion (L) core and (M) rim presented in K. (N) Same lesion presented in K showing sparse TMEM119 and CD206 double-positive cells within the lesion core (left side), whereas in the rim (right side), CD206⁺ cells are hardly present and TMEM119 single-positive cells prevail. (O and P) Higher magnification of lesion (O) core and (P) rim presented in N. (Q) In the core of stage II lesions, numerous CD163⁺ macrophages are present; similarly, CD163⁺ microglia are observed in the rim (R). Low numbers of TBB⁺ cells were found in the core (S) as well as in the lesion rim (T). Scale bars = 25 μm. Ctl = Control; C = Core; I–IV = stages; R = Rim.

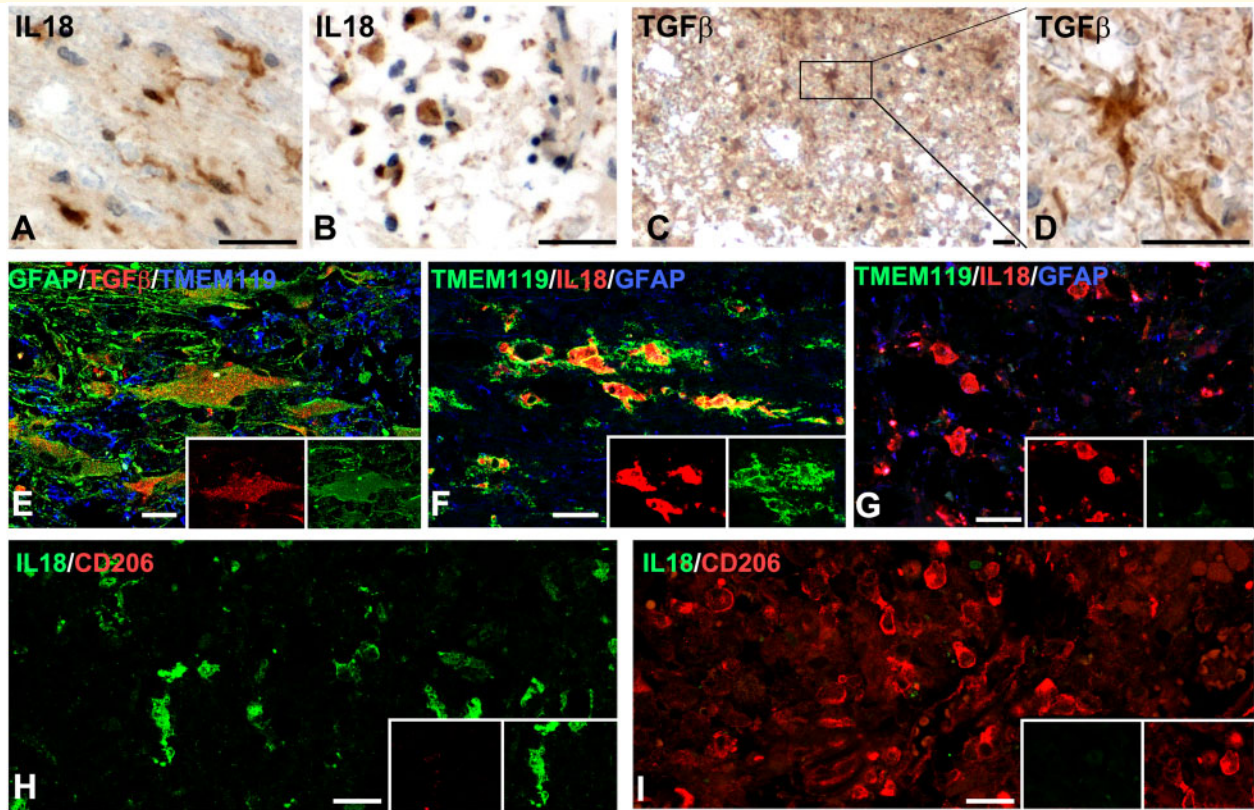


Figure 5 Cytokine expression in traumatic SCI. Numerous IL-18⁺ microglia and macrophages in the rim (A) and core (B) of SCI lesions. In contrast, TGF-β expression is restricted to astrocytes (C and D) in the lesion rim. Fluorescent triple stainings confirm TGF-β expression is restricted to GFAP⁺ astrocytes (E). Conformational triple stainings demonstrating IL-18 expression in TMEM119⁺ microglia in the rim (F) and in TMEM119⁻ macrophages in the core (G). While in the lesion rim pro-inflammatory IL-18⁺ microglia cells prevail (H), anti-inflammatory polarized CD206⁺ macrophages (I) are devoid of IL-18. All pictures are taken from stage II patients except C and D, which were taken from stage III. Scale bar = 25 μm.

together, our data indicate that the early inflammatory injury after traumatic SCI, which is accompanied by a disturbed neurovascular unit and a possible developing systemic coagulopathy (Maegle *et al.*, 2017), substantially differs from ischemic injury, particularly since the neurovascular unit evidently fails as a selective barrier for PMN infiltration after SCI.

Formation of two myeloid cell compartments after spinal cord injury

A crucial question is to what extent CNS-resident microglia and blood-derived myeloid cells contribute to the evolution further lesions (David and Kroner, 2011). Applying TMEM119, which has recently evolved as a marker exclusively expressed by microglia, we demonstrate that microglia were rapidly lost in the lesion core, while Iba-1⁺/TMEM119⁻ cells increased in this area. In contrast, within the rim a substantial proportion of Iba-1⁺ cells were derived from proliferating microglia cells in a similar percentage previously reported in mice (Greenhalgh and David, 2014).

This spatial segregation of different myeloid cell types mirrors exactly earlier reports studying bone marrow chimeric models (Popovich and Hickey, 2001). Infiltrating monocytes/macrophages have been suggested to stimulate remyelination (Kotter *et al.*, 2005; Miron and Franklin, 2014), while on the contrary an overall detrimental net effect of monocyte infiltration into SCI lesions on the recovery of the locomotor system has been demonstrated earlier (Popovich *et al.*, 1999). The net effect of microglia on neurological recovery remains unknown and is currently being investigated in pharmacological microglia ablation models. Of note, microglia deactivation resulted in the propagation of neurodegeneration after human CNS trauma suggestive of an at least partly protective role of microglia activation (Scott *et al.*, 2018).

After experimental SCI, polarization of myeloid cells towards an M2 phenotype has been associated with enhanced axonal outgrowth and improved recovery by attenuating inflammation (Kigerl *et al.*, 2009; Nakajima *et al.*, 2012; Kroner *et al.*, 2014). Generally, the M1/M2 paradigm may have to be dismissed in favour of a gradient of phenotypes between the both extremes M1 to M2. Particularly, the

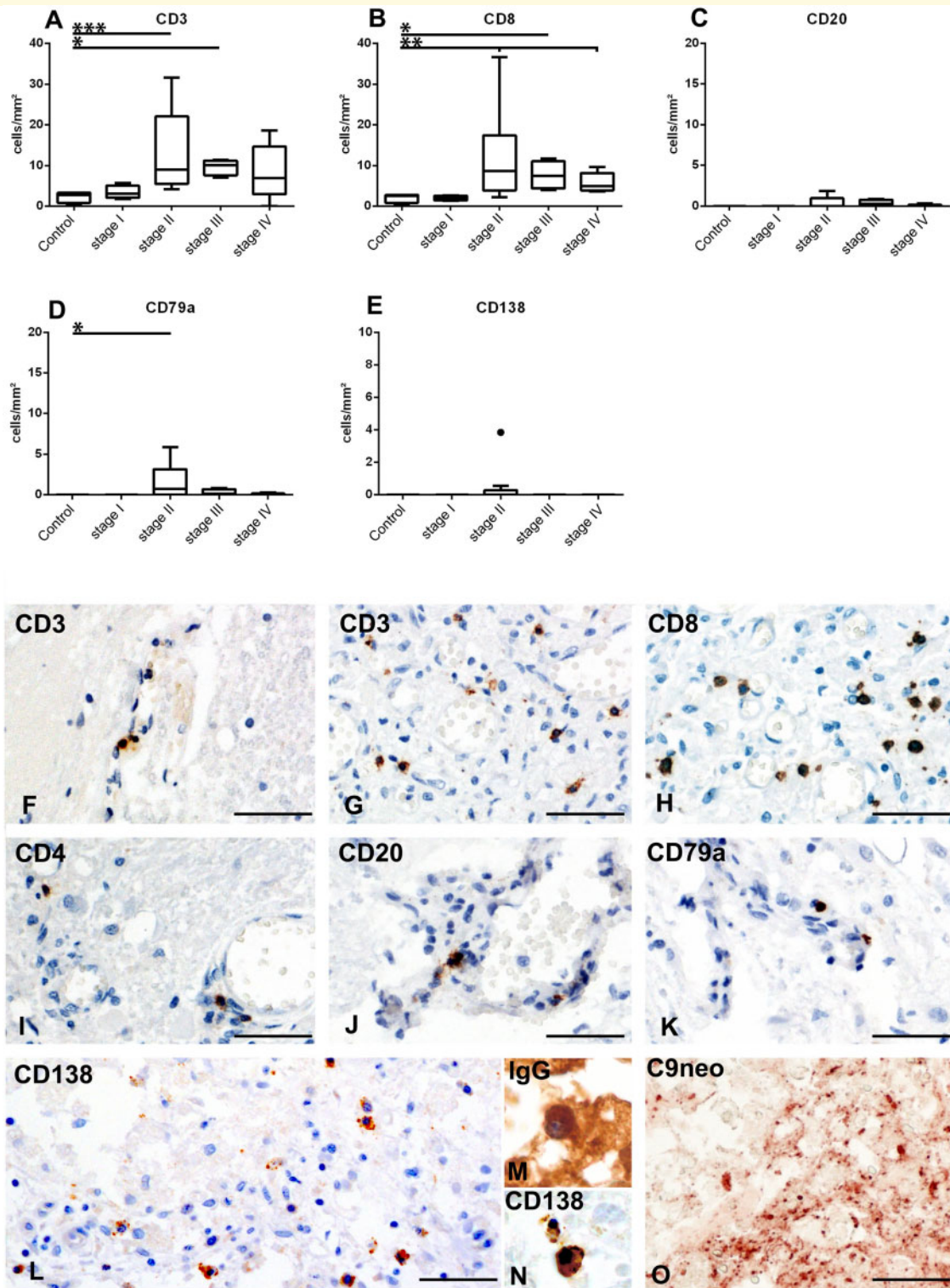


Figure 6 Moderate T cell and sparse B cell infiltration into the spinal cord after human traumatic SCI. Profile of total lymphocytes numbers populating the injured SCI over time. (A–E) Quantitation of the expression of the T cell markers CD3 (A) and CD8 (B), the B cell markers CD20 (C) and CD79a (D) and the plasma cell marker CD138 (E) in SCI lesions at different lesion stages (I–IV) compared with non-traumatic control tissue. Data represent numbers of cells/mm² **P* ≤ 0.05; ***P* ≤ 0.01; ****P* ≤ 0.001. (F) T cells were scarce, mostly perivascular, when observed in control patients. (G–I) Infiltrating CD3⁺ cells (G) in SCI are mainly MHC class I-restricted CD8⁺ cells (H), whereas only scattered CD4⁺ cells (I) were present in the injured neuropil. (J and K) Compared to T cells, single numbers of B cells mostly confined to perivascular areas were observed. (L–N) CD138⁺ plasma cells in a case of SCI was observed, which were identified as IgG positive plasma cells though double-labelling (N). (O) C9neo complement deposition of the same SCI case as in L–N. Scale bar = 25 μm.

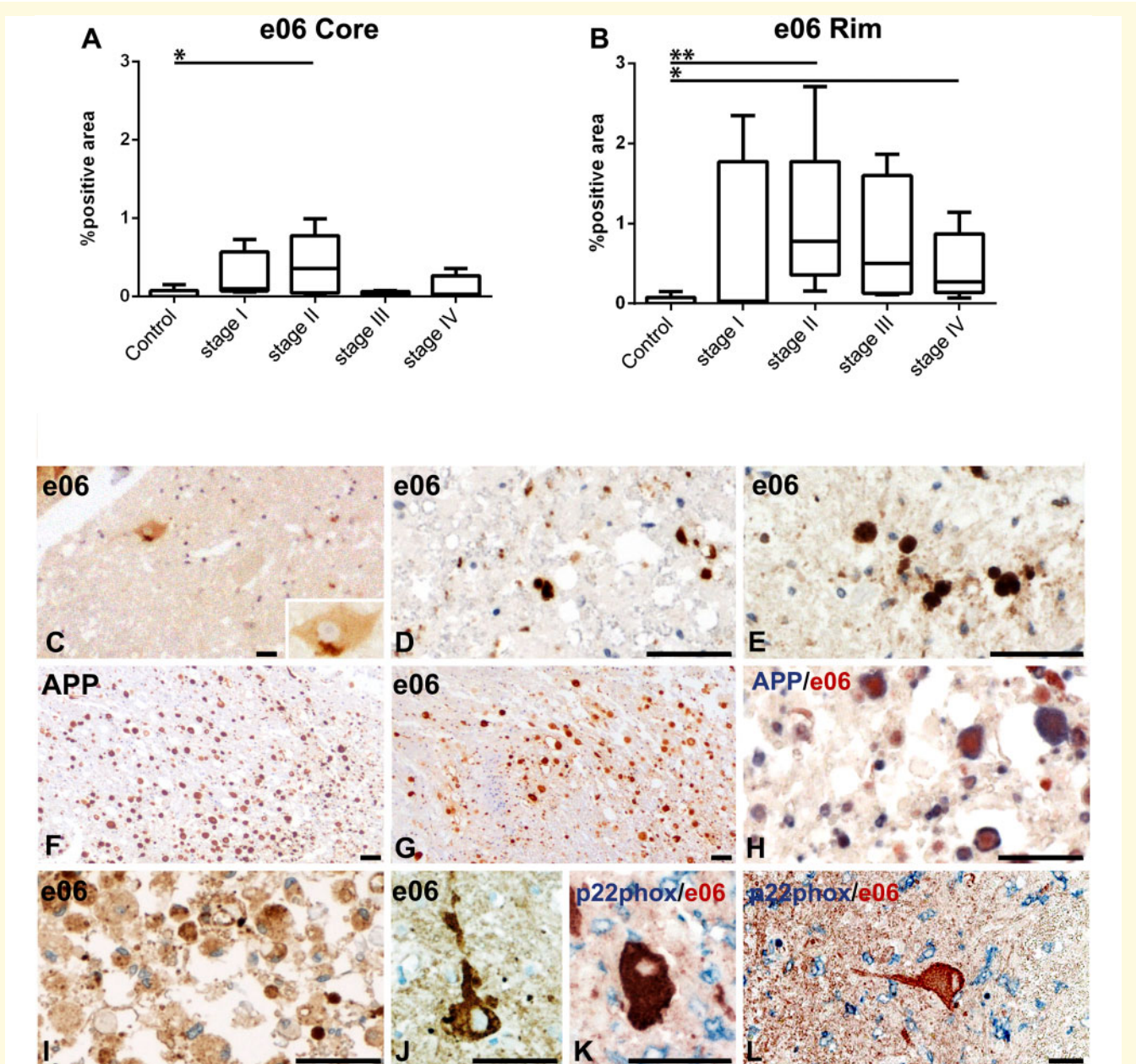


Figure 7 Oxidative injury after SCI affects spinal neurons. Presence of oxidized phospholipids (e06 immunoreactivity) in neurons has been associated with beading and fragmentation of cell processes in the human CNS (Fischer *et al.*, 2012) and occurs after SCI. (**A** and **B**) Percentage of positive area covered by e06 immunoreactivity within the lesion core (**A**) and lesion rim (**B**). (**C**) Immunoreactivity of e06 in lipofuscin granules in non-traumatic control spinal cords. (**D**) Few e06⁺ axonal bulbs within the lesion core during the first 3 days post-SCI (stage I). (**E**) Several e06⁺ axonal bulbs within the rim of chronic spinal cord lesions (stage IV). (**F**) At stage II, many APP⁺ axonal bulbs are present in the lesion rim, where oxidized phospholipids also accumulate (**G**). (**H**) Co-accumulation of oxidized phospholipids and APP in ballooned axonal spheroids and retraction bulbs. (**I**) Macrophages with granular cytoplasmic reactivity for oxidized phospholipids in the SCI core. (**J**) Intense e06 immunoreactivity in a neuron showing signs of degeneration and beading/fragmentation of cell processes. (**K**) Massive accumulation of oxidized phospholipids (e06⁺) in a degenerating neuron surrounded from and in contact with pro-inflammatory p22phox⁺ microglia (blue). (**L**) e06⁺ neuron undergoing central chromatolysis in contact with activated pro-inflammatory p22phox⁺ microglia. Scale bar = 25 μm.

characterization of phenotypes should include an extended panel of markers, since some traditional markers are not necessarily specific for the classical M1 or M2 phenotypes. For example, CD163, the haemoglobin-haptoglobin scavenger receptor, had originally been defined as an M2 marker but

was later found to be involved in other pathways as well (Van Gorp *et al.*, 2010). Furthermore, microglia in human disease conditions display mostly intermediate M1/M2 activation patterns as judged by the concomitant expression of pro- and anti-inflammatory markers (Vogel *et al.*, 2013;

Peferoen *et al.*, 2015; Zrzavy *et al.*, 2017, 2018, 2019). Finally, certain microglia functions, such as phagocytosis, had originally been defined as pro-inflammatory and disease promoting, but turned out afterwards to be essential in limiting the progression of tissue injury and in promoting tissue repair (Kotter *et al.*, 2005; Ulrich *et al.*, 2017). Thus, instead of strictly categorizing microglia and macrophage differentiation into M1 and M2, it seems more relevant to specifically define their functional properties. Here, we demonstrate that the homeostatic marker P2RY12 was promptly downregulated in a longstanding manner after SCI. Simultaneously, microglia/macrophages responded to the acute traumatic injury (Fleming *et al.*, 2006; Beck *et al.*, 2010; Krasemann *et al.*, 2017) with an upregulated expression of molecules involved in oxygen species generation (iNOS, p22phox), antigen presentation (MHC II), phagocytosis (enlarged CD68⁺ lysosomes) and increased levels of IL-18. This inflammatory pattern endures the early phases (stage I and II) and persists during the late sub-acute (stage III) and is evident even until chronic stages (stage IV) reflecting a chronic inflammatory state and possibly exacerbating of tissue injury. Prominent expression of CD163 in macrophages suggests that these cells are instrumental in the removal of haemoglobin from the lesion site; this is further supported by the detection of enhanced iron accumulation in a subset of macrophages/microglia. Accumulation of iron in oligodendrocytes, other glial cells and neurons, which in general occurs in the vicinity of haemorrhagic lesions in the brain (Hametner *et al.*, 2013; Glushakova *et al.*, 2014), was sparse or even absent in SCI lesions. Noteworthy, detection of interleukins via immunohistochemistry in archival formalin-fixed paraffin-embedded tissue is known to be challenging. However, the here applied panel of pro/anti-inflammatory cytokines has already been successfully applied in inflammatory CNS conditions (Machado-Santos *et al.*, 2018; Tröscher *et al.*, 2019), which is why we are confident that the absence of IL-1 β and IL-10 expression in myeloid cells is indeed representative.

Oxidative activation and oxidative injury after human spinal cord injury

Neuropathological studies have previously shown neuronal oxidative injury in inflammatory brain lesions in humans (Haider *et al.*, 2011; Fischer *et al.*, 2013). Experimental SCI studies indicate that reactive oxygen species produced by myeloid cells contribute to protracted tissue damage (Bao *et al.*, 2004; Pajooesh-Ganji and Byrnes, 2011). Here, we analysed the intracellular deposition of oxidative phospholipids via e06 immunohistochemistry as an established marker for oxidative injury (Haider *et al.*, 2011). This was prominently seen in the rim surrounding the necrotic core of the lesion. This indicates that oxidative injury is a major contributor of tissue damage, not only in the initial stages of

injury, but even progressing during the following months (Hausmann, 2003; Bastani *et al.*, 2012).

Lymphocytes are present during tissue remodelling and sustained injury

Lymphocytes have previously been described to populate the lesion site in comparatively low numbers after experimental SCI (Sroga *et al.*, 2003). Similarly, we only detected moderate numbers in our SCI cohort. A more detailed characterization revealed CD8⁺ T cells as the dominant lymphocyte population within spinal cord lesions. The dominance of CD8⁺ T cells is, however, not specific for SCI, but has already been seen in other inflammatory or neurodegenerative diseases of the human CNS. Even in the non-diseased brain the sparse parenchymal T cells compose of CD8⁺ over CD4⁺ cells. (van Nierop *et al.*, 2017; Machado-Santos *et al.*, 2018). Whether these cells play an active role in human SCI lesions or are passively recruited to the site of tissue damage remains unresolved.

Mice who are devoid of B cells showed better recovery after experimentally induced SCI (Ankeny *et al.*, 2009). Moreover, the production of auto-antibodies has been demonstrated in experimental models; injection of IgG fractions from SCI animals into naïve spinal cords subsequently triggered considerable neurotoxicity (Ankeny *et al.*, 2009). In humans, auto-antibodies directed against CNS antigens have been found in the serum after SCI (Hayes *et al.*, 2002; Zajarias-Fainsod *et al.*, 2012; for a review see Schwab *et al.*, 2014). In a previous study, B cells could not be detected in the affected areas after SCI in humans (Fleming *et al.*, 2006). In our study cohort comprising 22 SCI cases, we observed CD79a⁺ B cells and CD138⁺ plasma cells in the lesioned spinal cords in two patients. CD138⁺ plasma cells were IgG⁺ (Fig. 6L) indicating active antibody synthesis. Although B cells and plasma cells were very rare in the majority of SCI lesions, we nevertheless provide neuropathological evidence that, at least in a subpopulation of SCI patients: (i) B cells infiltrate the lesioned cord; (ii) convert into plasma cells; and (iii) begin to synthesize antibodies. Furthermore, complement deposition was observed within those and three additionally cases. Thus, B cell- and antibody-mediated neurotoxic immune mechanisms may contribute to tissue injury in a subset of SCI patients.

Several factors should be considered in the interpretation of our data. First, we do not have data on any treatment of our patients with methylprednisolone in the acute phase of injury. Methylprednisolone might have impacted on the inflammatory kinetics leading to a shift of the inflammatory response and potentially impacting on oxidative injury (Hall, 1993). If anything, it might have led to an attenuation of the acute inflammatory phase and thus, to an underestimation of the observed inflammatory neuropathology evident in our study cohort. As methylprednisolone is still occasionally applied to SCI patients, our findings might

represent the actual treatment situation and the actual pathology in ‘partly treated–partly untreated’ SCI patients very well. As another limitation of the study, it was not possible to determine in our SCI cohort, whether the degree of inflammation within the lesions was influenced by the severity of SCI as measured by the Asia Impairment Scale (AIS). A difference in AIS values within the four groups (stages I–IV) may modify the quantitative assessments but not the qualitative findings as such. We therefore refrained from further correlative analyses and focused on qualitative assessments. It should be noted that earlier reports (Fleming *et al.*, 2006) do not provide this information either.

Conclusion

Our data revise and amend the chronological order of pro- and anti-inflammatory cellular mediators upon traumatic SCI in humans. In this immunohistochemical study, we provide evidence for differing myeloid responses developing within the lesion core and the lesion rim post-SCI. The core mainly harbours blood-derived monocytes/macrophages, which further adopt an intermediate pro- and anti-inflammatory phenotype, while microglia within the rim locally proliferate and show a predominantly pro-inflammatory profile. Similarly, neuronal oxidative injury in the lesion core declines within months post-SCI, while it persisted in the lesion rims until the latest time points analysed (1.5 years post-SCI). The here-described long-lasting preservation of oxidative tissue injury might be a substantial contributor to (i) an impaired response to rehabilitation; (ii) overall failure of recovery; or (iii) delayed loss of recovered function. The different inflammatory cellular composition and activation in the lesion core compared with its rim results in distinct inflammatory milieus of relevance for topical cell transplantation, but also neuroprotective, or immunomodulatory interventions in SCI patients.

Acknowledgements

We thank Marianne Leißer, Ulrike Köck and Angela Kury for excellent technical assistance with immunohistological techniques.

Funding

This work was supported by grants from the Austrian Science Fund (FWF), Era-Net-NEURON Program (SILENCE; No. I 3334-B27) and the ‘Jubiläumsfonds der Österreichischen Nationalbank’, project 16919. J.M.S. received funding support from the Craig H. Neilsen Foundation (CHNF#596764), the Wings-for-Life Spinal Cord Research Foundation (#DE-047/14, DE-16/16); the Era-Net-NEURON Program of the European Union (EU) (SILENCE #01EW170A and SCI-Net #01EW1710); the

National Institute on Disability, Independent Living, and Rehabilitation Research (NIDILRR #90SI5020); and the W.E. Hunt & C.M. Curtis Endowment. J.M.S. is a Discovery Theme Initiative Scholar (Chronic Brain Injury) of the Ohio State University.

Competing interests

The authors report no competing interests.

Supplementary material

Supplementary material is available at *Brain* online.

References

- Ahuja CS, Wilson JR, Nori S, Kotter MR, Druschel C, Curt A, et al. Traumatic spinal cord injury. *Nat Rev Dis Primers* 2017; 3: 1–21.
- Ankeny DP, Guan Z, Popovich PG. B cells produce pathogenic antibodies and impair recovery after spinal cord injury in mice. *J Clin Invest* 2009; 119: 2990–9.
- Ankeny DP, Lucin KM, Sanders VM, McGaughy VM, Popovich PG. Spinal cord injury triggers systemic autoimmunity: evidence for chronic B lymphocyte activation and lupus-like autoantibody synthesis. *J Neurochem* 2006; 99: 1073–87.
- Bao F, Chen Y, Dekaban GA, Weaver LC. Early anti-inflammatory treatment reduces lipid peroxidation and protein nitration after spinal cord injury in rats. *J Neurochem* 2004; 88: 1335–44.
- Bao F, Chen Y, Schneider KA, Weaver LC. An integrin inhibiting molecule decreases oxidative damage and improves neurological function after spinal cord injury. *Exp Neurol* 2008; 214: 160–7.
- Bastani NE, Kostovski E, Sakhi AK, Karlens A, Carlsen MH, Hjeltnes N, et al. Reduced antioxidant defense and increased oxidative stress in spinal cord injured patients. *Arch Phys Med Rehabil* 2012; 93: 2223–8.e2.
- Bauer J, Lassmann H. Neuropathological techniques to investigate central nervous system sections in multiple sclerosis. *Methods Mol Biol* 2016; 1304: 211–29.
- Beck KD, Nguyen HX, Galvan MD, Salazar DL, Woodruff TM, Anderson AJ. Quantitative analysis of cellular inflammation after traumatic spinal cord injury: evidence for a multiphasic inflammatory response in the acute to chronic environment. *Brain* 2010; 133: 433–47.
- Bennett ML, Bennett FC, Liddel SA, Ajami B, Zamanian JL, Fernhoff NB, et al. New tools for studying microglia in the mouse and human CNS. *Proc Natl Acad Sci USA* 2016; 113: E1738–46.
- Bien CG, Vincent A, Barnett MH, Becker AJ, Blümcke I, Graus F, et al. Immunopathology of autoantibody-associated encephalitides: clues for pathogenesis. *Brain* 2012; 135: 1622–38.
- Butovsky O, Jedrychowski MP, Moore CS, Cialic R, Lanser AJ, Gabriely G, et al. Identification of a unique TGF-beta-dependent molecular and functional signature in microglia. *Nat Neurosci* 2014; 17: 131–43.
- David S, Kroner A. Repertoire of microglial and macrophage responses after spinal cord injury. *Nat Rev Neurosci* 2011; 12: 388–99.
- David S, Lopez-Vales R, Wee Yong V. Harmful and beneficial effects of inflammation after spinal cord injury: potential therapeutic implications. *Handb Clin Neurol* 2012; 109: 485–502.
- Dinkel K, Dhabhar FS, Sapolsky RM. Neurotoxic effects of polymorphonuclear granulocytes on hippocampal primary cultures. *Proc Natl Acad Sci USA* 2004; 101: 331–6.

- Dirnagl U. Modeling immunity and inflammation in stroke: can mice be trusted? *Stroke* 2014; 45: e177–8.
- Enzmann G, Mysiorek C, Gorina R, Cheng Y-J, Ghavampour S, Hannocks M-J, et al. The neurovascular unit as a selective barrier to polymorphonuclear granulocyte (PMN) infiltration into the brain after ischemic injury. *Acta Neuropathol* 2013; 125: 395–412.
- Fischer MT, Sharma R, Lim JL, Haider L, Frischer JM, Drexhage J, et al. NADPH oxidase expression in active multiple sclerosis lesions in relation to oxidative tissue damage and mitochondrial injury. *Brain* 2012; 135: 886–99.
- Fischer MT, Wimmer I, Höftberger R, Gerlach S, Haider L, Zrzavy T, et al. Disease-specific molecular events in cortical multiple sclerosis lesions. *Brain* 2013; 136: 1799–815.
- Fleming JC, Norenberg MD, Ramsay DA, Dekaban GA, Marcillo AE, Saenz AD, et al. The cellular inflammatory response in human spinal cords after injury. *Brain* 2006; 129: 3249–69.
- Freund P, Weiskopf N, Ashburner J, Wolf K, Sutter R, Altmann DR, et al. MRI investigation of the sensorimotor cortex and the cortico-spinal tract after acute spinal cord injury: a prospective longitudinal study. *Lancet Neurol* 2013; 12: 873–81.
- Friese MA, Schattling B, Fugger L. Mechanisms of neurodegeneration and axonal dysfunction in multiple sclerosis. *Nat Rev Neurol* 2014; 10: 225–38.
- Ginhoux F, Greter M, Leboeuf M, Nandi S, See P, Gokhan S, et al. Fate mapping analysis reveals that adult microglia derive from primitive macrophages. *Science* 2010; 330: 841–5.
- Glushakova OY, Johnson D, Hayes RL. Delayed increases in microvascular pathology after experimental traumatic brain injury are associated with prolonged inflammation, blood–brain barrier disruption, and progressive white matter damage. *J Neurotrauma* 2014; 31: 1180–93.
- Greenhalgh AD, David S. Differences in the phagocytic response of microglia and peripheral macrophages after spinal cord injury and its effects on cell death. *J Neurosci* 2014; 34: 6316–22.
- Gris D, Marsh DR, Oatway MA, Chen Y, Hamilton EF, Dekaban GA, et al. Transient blockade of the CD11d/CD18 integrin reduces secondary damage after spinal cord injury, improving sensory, autonomic, and motor function. *J Neurosci* 2004; 24: 4043–51.
- Haider L, Fischer MT, Frischer JM, Bauer J, Höftberger R, Botond G, et al. Oxidative damage in multiple sclerosis lesions. *Brain* 2011; 134: 1914–24.
- Haider L, Zrzavy T, Hametner S, Höftberger R, Bagnato F, Grabner G, et al. The topography of demyelination and neurodegeneration in the multiple sclerosis brain. *Brain* 2016; 139: 807–15.
- Hall ED. Neuroprotective actions of glucocorticoid and nonglucocorticoid steroids in acute neuronal injury. *Cell Mol Neurobiol* 1993; 13: 415–32.
- Hametner S, Wimmer I, Haider L, Pfeifenbring S, Brück W, Lassmann H. Iron and neurodegeneration in the multiple sclerosis brain. *Ann Neurol* 2013; 74: 848–61.
- Hausmann O. Post-traumatic inflammation following spinal cord injury. *Spinal Cord* 2003; 41: 369.
- Hayes KC, Hull TC, Delaney GA, Potter PJ, Sequeira KA, Campbell K, et al. Elevated serum titers of proinflammatory cytokines and CNS autoantibodies in patients with chronic spinal cord injury. *J Neurotrauma* 2002; 19: 753–61.
- James SL, Theadom A, Ellenbogen RG, Bannick MS, Montjoy-Venning W, Lucchesi LR, et al. Global, regional, and national burden of traumatic brain injury and spinal cord injury, 1990–2016: a systematic analysis for the Global Burden of Disease Study 2016. *Lancet Neurol* 2019; 18: 56–87.
- Jia Z, Zhu H, Li J, Wang X, Misra H, Li Y. Oxidative stress in spinal cord injury and antioxidant-based intervention. *Spinal Cord* 2012; 50: 264–74.
- Kerr BJ, Girolami EI, Ghasemlou N, Jeong SY, David S. The protective effects of 15-deoxy-delta-(12,14)-prostaglandin J2 in spinal cord injury. *Glia* 2008; 56: 436–48.
- Kigerl KA, Gensel JC, Ankeny DP, Alexander JK, Donnelly DJ, Popovich PG. Identification of two distinct macrophage subsets with divergent effects causing either neurotoxicity or regeneration in the injured mouse spinal cord. *J Neurosci* 2009; 29: 13435–44.
- Kirschblum S, Millis S, McKinley W, Tulsy D. Late neurologic recovery after traumatic spinal cord injury. *Arch Phys Med Rehabil* 2004; 85: 1811–7.
- Kotter MR, Zhao C, van Rooijen N, Franklin RJ. Macrophage-depletion induced impairment of experimental CNS remyelination is associated with a reduced oligodendrocyte progenitor cell response and altered growth factor expression. *Neurobiol Dis* 2005; 18: 166–75.
- Krasemann S, Madore C, Cialic R, Baufeld C, Calcagno N, El Fatimy R, et al. The TREM2-APOE pathway drives the transcriptional phenotype of dysfunctional microglia in neurodegenerative diseases. *Immunity* 2017; 47: 566–81.e9.
- Kroner A, Greenhalgh AD, Zarruk JG, dos Santos RP, Gaestel M, David S. TNF and increased intracellular iron alter macrophage polarization to a detrimental M1 phenotype in the injured spinal cord. *Neuron* 2014; 83: 1098–116.
- Machado-Santos J, Saji E, Tröscher AR, Paunovic M, Liblau R, Gabriely G, et al. The compartmentalized inflammatory response in the multiple sclerosis brain is composed of tissue-resident CD8+ T lymphocytes and B cells. *Brain* 2018; 141: 2066–82.
- Maegele M, Schochl H, Menovsky T, Marechal H, Marklund N, Buki A, et al. Coagulopathy and haemorrhagic progression in traumatic brain injury: advances in mechanisms, diagnosis, and management. *Lancet Neurol* 2017; 16: 630–47.
- Marino RJ, Ditunno JF Jr, Donovan WH, Maynard F Jr. Neurologic recovery after traumatic spinal cord injury: data from the Model Spinal Cord Injury Systems. *Arch Phys Med Rehabil* 1999; 80: 1391–6.
- Miron VE, Franklin RJ. Macrophages and CNS remyelination. *J Neurochem* 2014; 130: 165–71.
- Nakajima H, Uchida K, Guerrero AR, Watanabe S, Sugita D, Takeura N, et al. Transplantation of mesenchymal stem cells promotes an alternative pathway of macrophage activation and functional recovery after spinal cord injury. *J Neurotrauma* 2012; 29: 1614–25.
- Nguyen HX, O’Barr TJ, Anderson AJ. Polymorphonuclear leukocytes promote neurotoxicity through release of matrix metalloproteinases, reactive oxygen species, and TNF-alpha. *J Neurochem* 2007; 102: 900–12.
- Orr MB, Gensel JC. Spinal cord injury scarring and inflammation: therapies targeting glial and inflammatory responses. *Neurotherapeutics* 2018; 15: 541–53.
- Pajoohesh-Ganji A, Byrnes KR. Novel neuroinflammatory targets in the chronically injured spinal cord. *Neurotherapeutics* 2011; 8: 195–205.
- Peferoen LA, Vogel DY, Ummenthum K, Breur M, Heijnen PD, Gerritsen WH, et al. Activation status of human microglia is dependent on lesion formation stage and remyelination in multiple sclerosis. *J Neuropathol Exp Neurol* 2015; 74: 48–63.
- Popovich PG, Guan Z, Wei P, Huitinga I, van Rooijen N, Stokes BT. Depletion of hematogenous macrophages promotes partial hindlimb recovery and neuroanatomical repair after experimental spinal cord injury. *Exp Neurol* 1999; 158: 351–65.
- Popovich PG, Hickey WF. Bone marrow chimeric rats reveal the unique distribution of resident and recruited macrophages in the contused rat spinal cord. *J Neuropathol Exp Neurol* 2001; 60: 676–85.
- Pruss H, Kopp MA, Brommer B, Gatzemeier N, Laginha I, Dirnagl U, et al. Non-resolving aspects of acute inflammation after spinal cord injury (SCI): indices and resolution plateau. *Brain* 2011; 21: 652–60.
- Ramer LM, Ramer MS, Bradbury EJ. Restoring function after spinal cord injury: towards clinical translation of experimental strategies. *Lancet Neurol* 2014; 13: 1241–56.
- Ransohoff RM. A polarizing question: do M1 and M2 microglia exist? *Nat Neurosci* 2016; 19: 987–91.

- Satoh J, Kino Y, Asahina N, Takitani M, Miyoshi J, Ishida T, et al. TMEM119 marks a subset of microglia in the human brain. *Neuropathology* 2016; 36: 39–49.
- Schuh C, Wimmer I, Hametner S, Haider L, Van Dam A-M, Liblau RS, et al. Oxidative tissue injury in multiple sclerosis is only partly reflected in experimental disease models. *Acta Neuropathol* 2014; 128: 247.
- Schwab JM, Zhang Y, Kopp MA, Brommer B, Popovich PG. The paradox of chronic neuroinflammation, systemic immune suppression, autoimmunity after traumatic chronic spinal cord injury. *Exp Neurol* 2014; 258: 121–9.
- Scott G, Zetterberg H, Jolly A, Cole JH, De Simoni S, Jenkins PO, et al. Minocycline reduces chronic microglial activation after brain trauma but increases neurodegeneration. *Brain* 2018; 141: 459–71.
- Sroga JM, Jones TB, Kigerl KA, McGaughy VM, Popovich PG. Rats and mice exhibit distinct inflammatory reactions after spinal cord injury. *J Comp Neurol* 2003; 462: 223–40.
- Taoka Y, Okajima K, Uchiba M, Murakami K, Kushimoto S, Johno M, et al. Role of neutrophils in spinal cord injury in the rat. *Neuroscience* 1997; 79: 1177–82.
- Tröscher AR, Wimmer I, Quemada-Garrido L, Köck U, Gessl D, Verberk SG, et al. Microglial nodules provide the environment for pathogenic T cells in human encephalitis. *Acta Neuropathol* 2019; 137: 619–35.
- Ulrich JD, Ulland TK, Colonna M, Holtzman DM. Elucidating the role of TREM2 in Alzheimer's disease. *Neuron* 2017; 94: 237–48.
- Van Gorp H, Delputte PL, Nauwynck HJ. Scavenger receptor CD163, a Jack-of-all-trades and potential target for cell-directed therapy. *Mol Immunol* 2010; 47: 1650–60.
- van Nierop GP, van Luijn MM, Michels SS, Melief M-J, Janssen M, Langerak AW, et al. Phenotypic and functional characterization of T cells in white matter lesions of multiple sclerosis patients. *Acta Neuropathol* 2017; 134: 383–401.
- Vogel DY, Vereyken EJ, Glim JE, Heijnen PD, Moeton M, van der Valk P, et al. Macrophages in inflammatory multiple sclerosis lesions have an intermediate activation status. *J Neuroinflammation* 2013; 10: 35.
- Wardlaw JM, Benveniste H, Nedergaard M, Zlokovic BV, Mestre H, Lee H, et al. Perivascular spaces in the brain: anatomy, physiology and pathology. *Nat Rev Neurol* 2020; 16: 137–53.
- Williams PR, Marincu BN, Sorbara CD, Mahler CF, Schumacher AM, Griesbeck O, et al. A recoverable state of axon injury persists for hours after spinal cord contusion in vivo. *Nat Commun* 2014; 5: 5683.
- Zajarias-Fainsod D, Carrillo-Ruiz J, Mestre H, Grijalva I, Madrazo I, Ibarra A. Autoreactivity against myelin basic protein in patients with chronic paraplegia. *European spine journal: official publication of the European Spine Society, the European Spinal Deformity Society, and the European Section of the Cervical. Spine Res Soc* 2012; 21: 964–70.
- Ziegler G, Grabher P, Thompson A, Altmann D, Hupp M, Ashburner J, et al. Progressive neurodegeneration following spinal cord injury: implications for clinical trials. *Neurology* 2018; 90: e1257–e66.
- Zrzavy T, Hametner S, Wimmer I, Butovsky O, Weiner HL, Lassmann H. Loss of 'homeostatic' microglia and patterns of their activation in active multiple sclerosis. *Brain* 2017; 140: 1900–13.
- Zrzavy T, Höftberger R, Berger T, Rauschka H, Butovsky O, Weiner H, et al. Pro-inflammatory activation of microglia in the brain of patients with sepsis. *Neuropathol Appl Neurobiol* 2019; 45: 278–90.
- Zrzavy T, Machado-Santos J, Christine S, Baumgartner C, Weiner HL, Butovsky O, et al. Dominant role of microglial and macrophage innate immune responses in human ischemic infarcts. *Brain Pathol* 2018; 28: 791–805.